Power Management Circuit for Wireless Sensor Nodes Powered by Energy Harvesting: On the Synergy of Harvester and Load

Zheng Jun Chew, *Member, IEEE*, Tingwen Ruan, and Meiling Zhu, *Member, IEEE*

Abstract—**This paper presents an adaptive power management circuit which maximizes the energy transfer from the energy harvester to wireless sensor nodes in real world applications. Low power consumption techniques were adopted in the power management circuit to maximize the delivery of the harvested energy to the load instead of being consumed by the circuit. The presented circuit incorporates an analogue control circuit (ACC) for maximum power transfer from the energy harvester to the storage capacitor and an energy-aware interface (EAI) for controlling the energy flow from the storage capacitor to the load. To evaluate the performance of the presented circuit, piezoelectric energy harvesting was used as a studied case. The piezoelectric energy harvester (PEH) was mechanically excited at different strain loadings and frequencies. The experimental results show the circuit can self-start and powered directly by the PEH since the EAI and ACC have low power consumption in the range of micorwatts. The circuit is adaptive to energy harvesters of varying output and various electrical loads, with a peak efficiency of 76.18% in transferring the harvested energy from the PEH to the storage capacitor. More than 96% of the energy released from the storage capacitor is effectively transferred to the electrical load.**

Index Terms—**Adaptive power management, energy-aware interface, energy harvesting, IoT, low power consumption, maximum power transfer, wireless sensor node.**

I. INTRODUCTION

BATTERIES which are normally used to power small electronic devices have been recognized as a limiting factor for wide deployment of wireless sensor nodes (WSNs), especially in the vision of enabling the Internet of Things (IoT) because of their limited energy storage capacity and charge cycles [1]. Regular batteries replacement in the ever growing number of devices is an expensive and time consuming task. Moreover, the battery replacing work is non-trivial if the devices are embedded in difficult to access areas such as road tunnels and buildings [2]. Therefore, harvesting energy sources such as solar, heat, radio frequency (RF), and vibration from the ambient environments into electrical energy has been identified as one of the solutions for long term operation of the devices without the aforementioned limitations of batteries [3].

However, power densities of energy harvesters including RF rectennas, electromagnetic generators (EMGs), thermoelectric generators (TEGs), piezoelectric energy harvesters (PEHs), and photovoltaic (PV) cells are generally rated low at around 0.5 mW/cm^3 or less in their typical operating environments [4], [5]. This is because the output power of an energy harvester could be variable in amount and intermittent, depending on the surrounding conditions [6]-[8]. Although the output power can be increased by making the energy harvesters larger, there is usually a limit in practical implementation due to space constraint [5]. With the low harvested power, most of the energy harvesting powered systems are operating in a periodic manner to lower the average power consumption [3]. Also, the output from energy harvesters is rarely directly usable by WSNs. Therefore, in between the energy harvesters and loads which are both varying, adaptive power management circuits which consume very little of the harvested energy for their operation are required. The circuits need to manage the energy from the energy harvesters in a way that maximum amount of energy is transferred under various ambient conditions and convert the energy into a usable form for the WSNs.

Maximum power transfer occurs at maximum power point (MPP) of the energy harvesters. One of the most popular MPP finding methods is via fractional open-circuit voltage (FOCV). FOCV method samples the open-circuit voltage (V_{OC}) of the energy harvester first, and then determines the ratio of the V_{OC} which corresponds to the MPP of the energy harvester. It is an a priori technique based on many past analyses and experiments with the findings that the MPP for PV cells is around 0.71–0.82 of their V_{OC} [9], [10] while other types of energy harvesters such as RF rectennas [11], TEGs [6], PEHs [7], and EMGs [8], are around half of the open-circuit voltage ($V_{OC}/2$). The control circuits that find MPP using FOCV method are very low power, consuming around 100 nW to 10 μW [9]-[11] but might have slightly lower accuracy since FOCV does not require precise computation using microcontroller which usually consumes more power, for example, 408 μW [12]. Nevertheless, the low power consumption of the circuit is essential for an energy harvesting powered system because the end device may never start up if the power management circuit is power hungry, consuming most of the harvested energy. However, circuits using FOCV method have to be properly designed to withstand high V_{OC}, especially for PEHs because their V_{OC} can be more

than 100 V [13]. This will increase the size and cost of the circuit significantly [14], and possibly not viable due to voltage limitation of the fabrication technologies [15]. To avoid these problems, a method that directly finds the ratio of V_{OC} of the energy harvesters was proposed [16].

Apart from the MPP tracking capability, there are other factors that need to be considered as well to better utilize the harvested energy. For example, there are many circuits with high MPP tracking efficiency reported, but the harvested energy is stored in a capacitor which is placed at the output of the circuits [6], [7], [10]. The electrical load is connected directly to the output. Such a configuration inhibits the energy accumulation in the storage capacitor because energy is constantly drained by the electrical load. The drained energy is not enough to start up the WSN because the power required to initialize WSN could be two to three times higher than the power required for steady-state operation [17]. Some interfaces between the storage capacitor and the electrical load such as low-drop-out (LDO) regulators [9], dc–dc converters [8], and energy-aware interface [18] have been introduced to manage the energy flow. All these interfaces can be associated with low power consumption but they have different characteristics which may affect the energy transfer from the storage capacitor to the electrical load. For example, output voltage from LDOs and EAI cannot be higher than their input voltage while some dc–dc converters are able to output regulated voltage from much lower input voltage. Therefore, research on the energy transfer from an energy harvester to an electrical load by different circuit configurations is necessary to ensure maximum utilization of the harvested energy.

This paper presents an adaptive power management circuit to maximize the harvested energy for the use of the load using seamless control of MPP finding and energy flow management. The power management circuit can be powered up directly by the energy harvester for self-starting due to the low power consumption of the circuit. Piezoelectric energy harvesting will be used as a case study to evaluate the performance of the circuit. The circuit will be evaluated using different input vibrations and loads to verify its adaptiveness and operation. Apart from the system efficiency from the viewpoint of power, energy flow versus time analysis involving energy harvesting, charging and discharging of energy storage is presented since powering a load via energy harvesting is a time-related process. The circuit will be evaluated using different input vibrations and resistive loads to verify its adaptiveness and operation. The amount of energy that can be utilized by a load using the proposed circuit will be compared with other circuit architectures to assess the advantage of the presented circuit in allowing better utilization of the harvested energy by the load.

II. SYSTEM DESCRIPTION

The studied system architecture for the energy harvesting power management circuit is composed of five main subsystems, namely a full-wave diode bridge (FB) rectifier for converting the ac output from the PEH into a dc output, an analogue control circuit (ACC) for performing the MPP finding, a dc–dc converter as part of the subsystem for the MPP finding and for transferring energy from the PEH to a storage capacitor, a storage capacitor for accumulating the harvested energy and supplying the energy to the load, and an EAI for energy flow management between the storage capacitor and the load, as shown in Fig. 1 [19]. The key subsystems are the ACC and the EAI which will be explained in this section. The operation of the whole power management circuit will be also explained here. It should be noted that the ACC and dc–dc converter have to work together, and therefore they can be regarded as a power management module (PMM) here. Also, the rectifier is only needed for energy harvesters with ac output.

A. Maximum Power Transfer from Energy Harvester

The ACC finds the MPP of an energy harvester based on the well-known principle that maximum power transfer occurs at certain fraction of the V_{OC} of the energy harvester, depending on its type as mentioned earlier in the Introduction. Its operational principle is briefly explained below.

Unlike many conventional methods that involve a two-step process of finding V_{OC} first, the ACC exploits the RC response of a charging capacitor to directly determine $V_{OC}/2$ of an energy harvester using a specifically designed high-pass filer [16]. The ACC tracks the voltage charging profile of the rectified voltage $V_{rect\text{-}PMM}$ at the smoothing capacitor C_i which is charged up by the rectified PEH in this studied case until the output voltage of the high-pass filter reaches its peak, indicating that $V_{OC}/2$ of the PEH has been found as illustrated in Fig. 2.

To achieve this, the dc–dc converter is disabled initially, and can be regarded as open-circuited to the PEH. The PEH and FB rectifier can be seen as a dc voltage source which charges up capacitor C_i. Therefore, they can be modelled as an equivalent RC circuit model, that is, a dc voltage source with the magnitude $|V_{OC}|$ and the equivalent series resistance with the magnitude R_e to charge up the smoothing capacitor C_i as shown in Fig. 1. Assume that the FB rectifier is lossless, voltage $V_{rect\text{-}}$
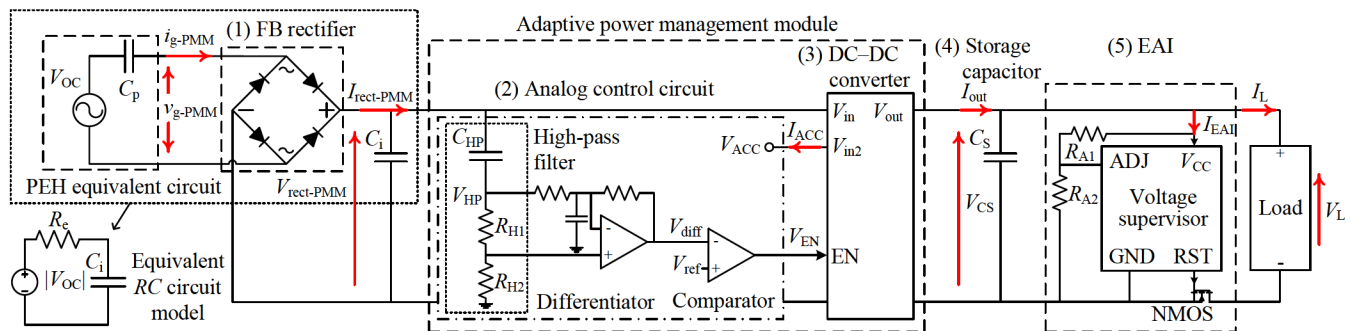

Fig. 1. Schematic circuit diagram of the studied power management circuit.

PMM will gradually increase towards V_{OC} of the PEH.

The high-pass filter is formed by C_{HP}, R_{H1}, and R_{H2}, which have been designed to have its output V_{HP} peaks when $V_{rect-PMM}$ is equal to $V_{OC}/2$. This is achieved by setting the time constant τ_{HP} of the high-pass filter to be the same as the time constant τ_{RC} of the equivalent RC circuit formed by the rectified PEH, FB rectifier, and C_i. The time constant τ_{HP} of the high-pass filter is equal to $C_{HP}(R_{H1}+R_{H2})$ and the time constant τ_{RC} is equal to R_eC_i of the equivalent RC circuit [16].

The peak of V_{HP} can be determined by using a differentiator since derivative of maxima is zero. A comparator compares the output from the differentiator V_{diff} at its negative input with a reference voltage V_{ref} which is slightly away from zero at its positive input. This is because in practice, it is difficult for a comparator to compare a zero value with a reference which is zero as well where the output can be unpredictable. Once V_{diff} drops below V_{ref}, the comparator sends out a signal pulse V_{EN} to enable the dc–dc converter for energy transfer from the PEH to the storage capacitor. With the energy transfer started, $V_{rect-PMM}$ will decrease and cause V_{HP} and subsequently V_{diff} to change. The changes take some time due to the RC nature of the circuit, which gives enough time for the energy transfer. The dc–dc converter will then be disabled and the whole cycle repeats.

B. Energy Flow Management

In the energy flow management, the main function of the EAI is to ensure that the harvested energy can be accumulated in the storage capacitor until there is sufficient energy for the operation of the end device, before allowing the end device to draw any energy from the storage capacitor. This means no energy will be used by the end device when the energy is insufficient to allow for the energy accumulation. Operation of the EAI can be explained using voltage of the storage capacitor since energy can be related to voltage via $\frac{1}{2}CV^2$.

The EAI comprises a voltage supervisor to monitor V_{CS} and an N-channel MOSFET (NMOS) as a switch, as shown in Fig. 1 [18]. The turn-on threshold $V_{CS,H}$ and the turn-off threshold $V_{CS,L}$ has to be set at the voltage supervisor according to the requirement of the load to be powered. $V_{CS,H}$ is usually a voltage sufficiently high for the operation of the load without exceeding the maximum operating voltage of the load and the output voltage from the dc–dc converter [20]. $V_{CS,L}$ is usually a voltage near to the minimum operating voltage of the load.

Fig. 3 illustrates the changes of the voltage V_{CS} at the storage capacitor as controlled by the EAI. Assuming that the storage capa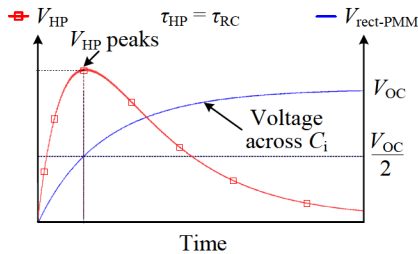citor is completely discharged initially, V_{CS} gradually increases from 0 V as energy is being accumulated in the storage capacitor which is charged up by the energy harvester via the dc–dc converter. Once V_{CS} reaches $V_{CS,H}$, the load will be connected to the storage capacitor as the voltage supervisor turns on the NMOS via its RST pin, connecting the negative terminal of the load to the system ground. Therefore, the load and the storage capacitor form a closed circuit which allows energy from the storage capacitor to be drawn by the load.

V_{CS} will drop as the load is discharging the storage capacitor. When V_{CS} decreases to $V_{CS,L}$, the voltage supervisor turns off the NMOS to disconnect the load from the storage capacitor to stop the load from discharging the capacitor. This is to prevent energy wastage since the load cannot operate properly once the voltage has dropped below its minimum operating voltage but it will still draw energy from the capacitor which decreases V_{CS}. The capacitor can then be recharged in a shorter time from $V_{CS,L}$ to $V_{CS,H}$ to power the load sooner and the whole cycle repeats.

The EAI is also functioning as a voltage limiter since it releases energy from $V_{CS,H}$ to $V_{CS,L}$ that are appropriate voltage levels within the operating voltage range of the load. It should be noted that the energy is directly transferred to the load from the storage capacitor via the NMOS instead of having to go through a more complicated circuit such as a LDO or dc–dc converter. This makes the energy transfer from the storage capacitor to the load more efficient as energy does not have to be dissipated by a complex system before reaching the load.

C. Operation of the Proposed Power Management Circuit

The circuit has three operating stages in charging up the storage capacitor to a voltage of $V_{CS,H}$ and discharging of the storage capacitor to a voltage of $V_{CS,L}$. Simplified circuit diagrams and main waveforms of the circuit are shown in Figs. 4 and 5, respectively to help the explanation of the circuit operation. Greyed out functional blocks in Fig. 4 are either disabled or uninvolved in that operating stage, which leads to low power consumption as they are not active all the time.

Stage 1 is that the dc–dc converter has been disabled by the ACC where the dc–dc converter and any circuitries beyond as seen by the rectified PEH can be regarded as open-circuited. With the load which could be highly dynamic decoupled from the PEH, its influence on the PEH is removed. Without the loading effect from the load, smoothing capacitor C_i can be charged up to $V_{OC}/2$ of the PEH as shown in Fig. 5. The ACC monitors the changes of $V_{rect-PMM}$ as explained in Section II.A.

Stage 2 is that once $V_{rect-PMM}$ is equal to $V_{OC}/2$, the ACC sends a HIGH V_{EN} to enable the dc–dc converter for energy transfer
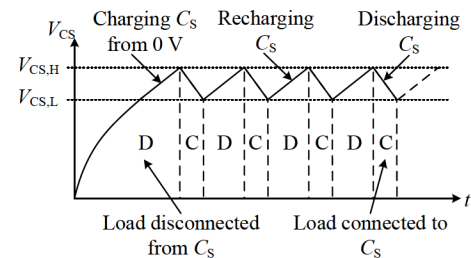

Fig. 2. Illustration of V_{HP} which peaks at the time when $V_{rect-PMM}$ equals $|V_{OC}|/2$ of the PEH with the RC time constants of the high-pass filter formed by C_{HP}, R_{H1}, and R_{H2} set to be the same as the RC time constant of the equivalent RC circuit formed by the rectified PEH, FB rectifier, and C_i.

Fig. 3. Illustration of V_{CS} across the storage capacitor C_S as controlled by the EAI, where the letter 'D' indicates that the load is disconnected from the capacitor to allow energy accumulation in C_S and 'C' indicates that the load is connected to the storage capacitor to use the stored energy and discharge C_S.

from the PEH to the storage capacitor. $V_{\text{rect-PMM}}$ will drop below $V_{\text{OC}}/2$ while V_{CS} increases following the energy transfer. Therefore, the circuit will go back to Stage 1 with the dc–dc converter disabled again until $V_{\text{rect-PMM}}$ reaches $V_{\text{OC}}/2$.

The power management circuit operates alternately between Stage 1 and Stage 2 until the storage capacitor C_{S} is charged up to $V_{\text{CS,H}}$. In both Stages 1 and 2, the EAI monitors V_{CS} and by default is assumed to disconnect the load from the storage capacitor so that energy can be accumulated.

Stage 3 is that once V_{CS} has reached $V_{\text{CS,H}}$, RST of the voltage supervisor becomes HIGH to turn on the NMOS for the load to be connected to the system ground, forming a closed-circuit with the storage capacitor to allow energy flowing to the load. Voltage V_{L} across the load is now equal to voltage V_{CS}. When V_{CS} drops to $V_{\text{CS,L}}$, RST becomes LOW, which turns off the NMOS and disconnects the load from the storage capacitor.

It should be noted that the energy transfer process from the PEH is still ongoing during Stage 3. This means Stage 1 or Stage 2 may occur simultaneously with Stage 3 depending on the voltage level of $V_{\text{rect-PMM}}$, and their default state of having the load disconnected will become connected to C_{S} during this concurrent stages. The circuit will go back to either the default state of only Stage 1 or 2 depending on the voltage level of $V_{\text{rect-PMM}}$ when V_{CS} reaches $V_{\text{CS,L}}$, and the whole cycle repeats.

III. SYSTEM IMPLEMENTATION

This section discusses the implementation of the ACC and EAI, and also the selection of the rectifier, dc–dc converter, load to simulate a WSN, and size of storage capacitor in this circuit to ensure the whole circuit works in an intended manner.

A. Power Management Module

The PMM is formed by a dc–dc converter and the ACC. The dc–dc converter was chosen based on the output voltage of the energy harvester. Since PEHs are normally characterized by high voltage and low current, a LTC3388-3 buck converter was chosen. It steps down the high voltage from PEHs to a low voltage of up to 3.3 V that is suitable for low power electronics and converts the low current from PEHs into a higher current to quickly charge up the energy storage devices such as
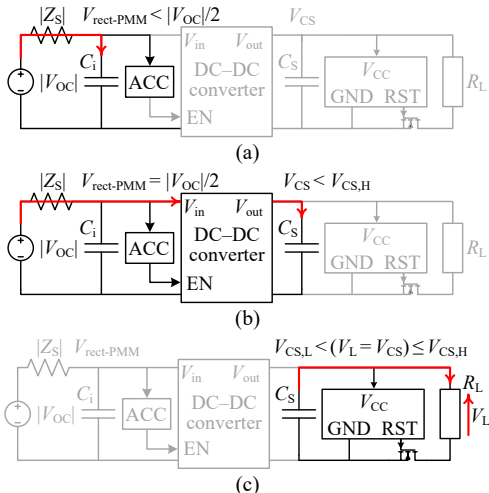
supercapacitors that usually have low operating voltage. The internal rail voltage V_{in2} of LTC3388-3 is used to power the ACC. V_{in2} follows the voltage of the PEH initially but will become steady at 4.6 V once the voltage of the PEH becomes higher than 4.6 V regardless of whether the dc–dc converter is enabled or not. The ACC is built from low power operational amplifier (LPV521) for the differentiator and comparator (LTC1540) to enable or disable the dc–dc converter.

B. Energy-Aware Interface

The EAI was implemented using a low power voltage supervisor (LTC2934-2) and an NMOS as discussed earlier in Section II.B. $V_{\text{CS,H}}$ and $V_{\text{CS,L}}$ were set by selecting appropriate R_{A1} and R_{A2} in mega-ohms range to minimize loss. The resistors were connected to the ADJ pin of the voltage supervisor [21] as shown in Fig. 1. $V_{\text{CS,L}}$ can also be set using external control where the voltage supervisor can switch off the NMOS before V_{CS} drops to the hardware configured $V_{\text{CS,L}}$ by applying a LOW signal to the MR pin of the voltage supervisor [21]. This offers flexibility to the application where the end device can send a LOW signal to the MR pin as soon as it finishes its tasks.

C. Rectification Circuit

A FB rectifier was used due to its simplicity without the need of any control circuit and robustness over a wide range of input voltage. Given that the output voltage from the PEH can be much higher than the forward voltage drop of a diode and the current from the PEH flowing through the diode is low, the power dissipated by a diode-based rectifier can be low. BAS70 Schottky diodes were chosen to build the FB rectifier in this circuit for their low reverse current and forward voltage drop.

D. Resistive Load to Emulate a Wireless Sensor Node

Voltage across a capacitor drops when a device such as a WSN consumes energy from the capacitor. This is similar to using a resistor to discharge a capacitor. Therefore, a resistor was used to emulate a WSN for simplicity. In this study, the storage capacitor will be discharged from 3.28–2.0 V, since many microcontrollers used in WSNs are operational over a large voltage range from 1.8–3.8 V [15], [22]. ZigBee nodes are commonly used and they consume an average current of 5 mA during active operations [22]. Therefore, a 500 Ω resistor was chosen since it would draw an average current of approximately
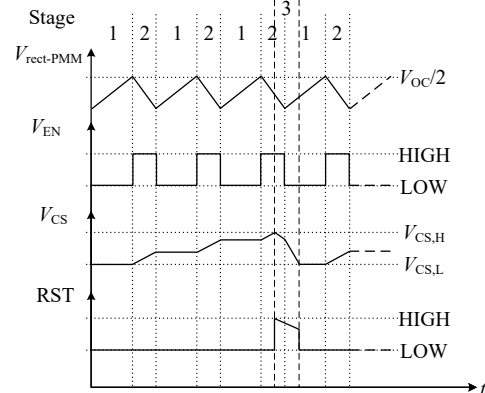

Fig. 4. Illustrations of the operating stages of the power management circuit: (a) Stage 1, (b) Stage 2, and (c) Stage 3.

Fig. 5. Main waveforms of the circuit in one charging and discharging cycle of the storage capacitor.

5 mA from the storage capacitor as V_{CS} drops from 3.28–2.0 V.

E. Storage Capacitor

In real world applications, a WSN would normally be turned on for a period of time to perform all the necessary tasks, such as data reading from sensors, data processing, data storing, and data transmission or receiving in an active cycle before going into the non-active phase when the voltage at the storage capacitor drops to a low level of $V_{CS,L}$. The value of C_S can be chosen based on the energy needed for the period of operation and calculated by rearranging the capacitor discharging equation as shown in (1) get (2).

$$V_{CS,L} = V_{CS,H} e^{\frac{-t}{R_L C_S}} \tag{1}$$

$$C_S = \frac{-t}{R_L \ln\left(\frac{V_{CS,L}}{V_{CS,H}}\right)} \tag{2}$$

By assuming that the WSN can stay active for a period of time to perform its required tasks, for example, 5 s, a suitable value of C_S can be obtained by substituting the implemented system parameters of $t = 5$ s, $R_L = 500$ Ω, $V_{CS,H} = 3.28$ V, and $V_{CS,L} = 2.0$ V into (2). C_S is found to be 20 mF using these parameters. Taking into account the possible tolerance of a capacitor, a 22 mF supercapacitor was chosen for all the tests.

IV. Experimental Verification Approaches

To evaluate the performance of the proposed circuit, a prototype was built and tested using commercially available discrete components on a printed circuit board, as shown in Fig. 6. The experimental setup and evaluation methods of the system performances are detailed as follows.

A. Experimental Setup

A commercially available macro fibre composite (MFC) M8528-P2 from Smart Material bonded on a piece of carbon fiber composite material using adhesive glue was used as the PEH in this experiment [23]. An Instron E10000 ElectroPuls dynamic testing machine was used to apply different strain loadings at different frequencies onto the PEH. The PEH was mounted in the Instron machine using the grips as shown in Fig. 7, where the bottom grip is fixed while the top grip is movable. Therefore, the output from the PEH is sinusoidal due to the cyclic movement of the grips. An extensometer was mounted to measure the strain waveform applied onto the PEH.

Besides the proposed circuit shown in Fig. 1, two additional circuits were used to evaluate the performances of the proposed circuit. The circuit in Fig. 8(a) is similar to the proposed circuit but it uses two dc–dc converters based on the topology in [8] without the EAI, where one is for charging the storage capacitor just as the proposed circuit and another one is for delivering energy to the load. It serves as a reference to evaluate the energy flow management of the EAI in the proposed circuit. Fig. 8(b) is a circuit that uses a variable resistor to replace the circuitry after the smoothing capacitor C_i, serving as a reference to determine the MPP finding capability of the proposed circuit. The resistance of the variable resistor R_L was manually tuned until the maximum generated power was obtained in each test.

Voltage and current measurements of the PEH were made using a National Instrument (NI) data acquisition system (DAQ) with NI 9229 modules while other measurements were made using a number of Keithley 2612B sourcemeters (SMUs). It should be noted that the NI 9229 can measure voltages only. Therefore, the current i_g generated by the PEH was obtained by measuring the voltage across a small sensing resistor R_{sense} of 20 Ω in series with the PEH. The NI DAQ system and SMUs were all connected to a computer to record all the measurements directly into the computer.

B. Energy Harvesting Capability Under Different Vibrations

Three sets of peak-to-peak strain loadings at 300 $\mu\varepsilon$, 400 $\mu\varepsilon$, and 500 $\mu\varepsilon$ with frequencies of 2, 4, 6, 8, and 10 Hz were applied onto the PEH to verify the capability of the proposed circuit in adapting to variable input energy due to vibrations of different amplitudes and frequencies. Voltage and current of the PEH were measured. The load resistance R_L at the output of the proposed circuit was fixed at 500 Ω for the energy harvesting capability testing. The tests were repeated by using the circuit in Fig. 8(b) with R_L tuned to its optimal value. The power generated by the PEH using both circuits was compared.

C. Adaptability to Connected Electrical Loads

A WSN draws different amount of currents at different operation modes [22]. This means a WSN can be seen as a load
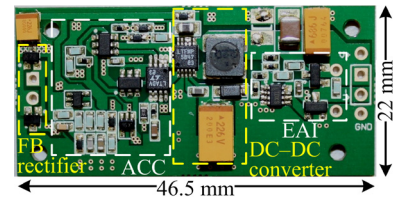

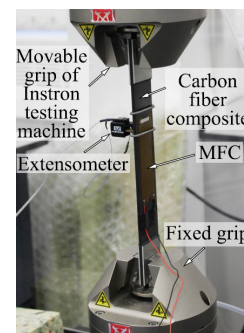Fig. 6. Prototyped circuit with the subsystems highlighted.

Fig. 7. Image of the PEH held by the grips of the Instron testing machine which applies mechanical loadings of different strains and frequencies onto the PEH.
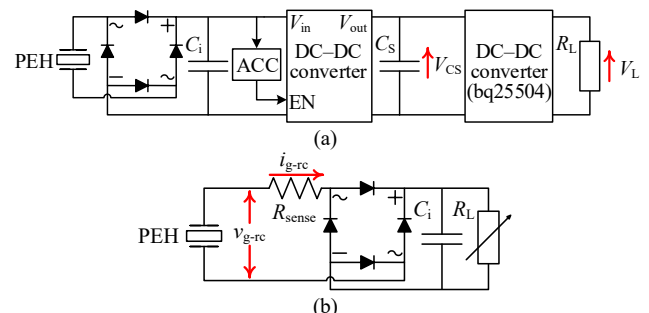

Fig. 8. Schematic diagrams of (a) circuit with two dc–dc converters without EAI and (b) circuit with RC load with their measurement points.

with a time-varying resistance by the power management circuit at different operation modes of the WSN. Ideally, the proposed circuit is required to be able to harvest the maximum possible power from the energy harvester without the influence of the connected load. In this experiment, different values of R_L at 100 Ω, 1 kΩ, 10 kΩ, and 100 kΩ were used to evaluate the performance of the proposed power management circuit in harvesting energy regardless of the connected load. The same three sets of strain loadings at 300 με, 400 με, and 500 με with vibrational frequency of 10 Hz were used for the evaluation.

D. Performance of the Overall System and Subsystems

To evaluate the efficiencies and losses of the overall system and individual subsystems, power generated and power consumed by different parts of the power management circuit were measured and analyzed. The instantaneous power p_g generated by the PEH is the product of the measured voltage v_g and current i_g as given in (3). The average power P_g was calculated using (4).

$$p_g(t) = v_g(t) i_g(t) \qquad (3)$$

$$P_g = \frac{1}{T} \int_0^T p_g(t)\,dt \qquad (4)$$

The power generated by the PEH in the proposed power management circuit and the circuit with an RC load in Fig. 8(b) is distinguished by adding the subscripts 'PMM' and 'rc' which represent the two different circuit configurations connected at the rectifier output. The average power $P_{rect-PMM}$ after the rectifier, power consumptions P_{ACC} and P_{EAI} of the ACC and the EAI, respectively, and output power P_{out} of the dc–dc converter were measured by the SMUs and calculated using (5).

$$P_x = \frac{\sum_{k=1}^{N} V_x(k) I_x(k) \Delta t}{t(N)} \qquad (5)$$

where the subscript x represents the relevant parts of the systems, such as 'rect-PMM' and 'ACC' for the rectifier and analog control circuit, respectively. P_{out} and P_{EAI} were obtained by multiplying V_{CS} with I_{out} and I_{EAI}, respectively. Δt is the

sampling time interval of the SMUs and $t(N)$ is the total sampling time for the measurement.

The rectifier efficiency η_{rect} is the ratio of $P_{rect-PMM}$ to P_{g-PMM} as given by (6). Power dissipated by the FB rectifier P_{FB} is the difference between P_{g-PMM} and $P_{rect-PMM}$ as given by (7).

$$\eta_{rect} = \frac{P_{rect-PMM}}{P_{g-PMM}} \qquad (6)$$

$$P_{FB} = P_{g-PMM} - P_{rect-PMM} \qquad (7)$$

The efficiency of the PMM which consists of the ACC and dc–dc converter η_{PMM} is defined as the ratio of P_{out} to $P_{rect-PMM}$ as given by (8). The power consumed and loss at the dc–dc converter P_{DCDC} is the difference between its input power and output power. Since part of the $P_{rect-PMM}$ is consumed by the ACC, which is not used by the dc–dc converter, P_{ACC} has to be deducted from $P_{rect-PMM}$ in the calculation as given by (9).

$$\eta_{PMM} = \frac{P_{out}}{P_{rect-PMM}} \qquad (8)$$

$$P_{DCDC} = P_{rect-PMM} - P_{ACC} - P_{out} \qquad (9)$$

The ratio of the amount of power available to the load to the power from the PEH is the metric used to determine the overall system efficiency. The overall system efficiency in delivering the harvested power to the load is therefore the ratio of P_{out} minus P_{EAI} to P_{g-PMM} as given by (10) since part of the power at the output of the dc–dc converter is consumed by the EAI.

$$\eta_{overall} = \frac{P_{out} - P_{EAI}}{P_{g-PMM}} \qquad (10)$$

V. RESULTS AND DISCUSSIONS

A. Validation of the Circuit Operation

Fig. 9 shows the measured v_{g-PMM} and V_{CS} when the PEH was subjected to a peak-to-peak strain level of 500 με at 10 Hz as an example. It can be seen that V_{CS} gradually increases from 0 V as energy is transferred from the PEH to the storage capacitor, which is known as the charging phase. When V_{CS} reaches around 3.28 V, the storage capacitor is discharged by the 500 Ω resistor, controlled by the EAI as explained in Section II.B. Once V_{CS} drops to around 2.0 V, the resistive load is disconnected from the storage capacitor by the EAI to allow the
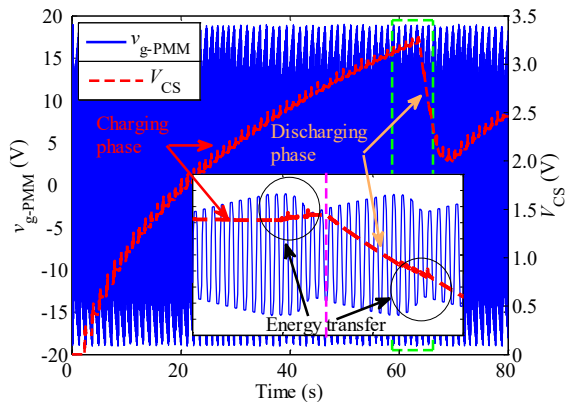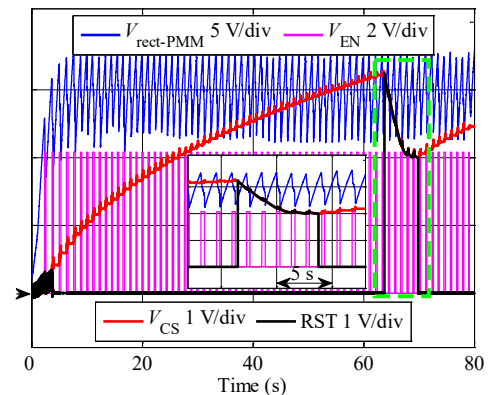

Fig. 9. Measured v_{g-PMM} and V_{CS} of the proposed power management circuit. Inset shows the enlarged view of the area highlighted by the dashed line where v_{g-PMM} is not affected by the states of V_{CS} which is either being charged (load disconnected) or discharged (load connected).

Fig. 10. Measured $V_{rect-PMM}$, V_{EN}, V_{CS}, and RST of the proposed power management circuit, showing its operation in transferring energy from an energy harvester to a storage capacitor and releasing the energy to a load. Inset shows the enlarged view of the area highlighted by the dashed line.

storage capacitor to be recharged again.

The area enclosed by the dashed lines in Fig. 9 is enlarged in the inset. It can be seen that when energy is transferred, there will be a decrease in $v_{\text{g-PMM}}$ and increase in V_{CS}. The waveform profile of $v_{\text{g-PMM}}$ remains the same in both the charging and discharging phases. This shows that the energy transfer of the proposed power management circuit is unaffected by the connected load during the discharging process. This attribute is due to the implemented operation as described in Section II.C which decouples the PEH from the dc–dc converter and the load until sufficient energy has been accumulated for the load.

Fig. 10 shows the measured $V_{\text{rect-PMM}}$, V_{EN}, V_{CS}, and RST, validating the circuit operation. $V_{\text{rect-PMM}}$ gradually increases and once $V_{\text{rect-PMM}}$ reaches the voltage level which corresponds to $V_{\text{OC}}/2$ as determined by the ACC, V_{EN} becomes high to enable the dc–dc converter for energy transfer. Since the energy is transferred and stored in the storage capacitor, V_{CS} increases while $V_{\text{rect-PMM}}$ decreases. After the energy transfer process, $V_{\text{rect-PMM}}$ increases again and the whole cycle repeats. Once V_{CS} reaches 3.28 V, RST becomes high to allow the energy stored to be discharged by the load. RST remained high as the capacitor is discharged by the load until V_{CS} drops to 2.0 V. Then, RST will become low again to stop the energy stored in the capacitor from being further discharged. Energy can now be accumulated in the storage capacitor again until V_{CS} reaches the turn-on threshold voltage for powering the load. The circuit can

be seen to self-start without issue as the ACC can start sending pulses to initiate the energy transfer almost immediately. In the inset of Fig. 10, it can be seen that V_{EN} is consistent regardless of the state of RST. This means the operations of the ACC and EAI do not interrupt each other, ensuring a seamless energy transfer from the energy harvester to storage, and to the load.

Fig. 11 shows the voltages across the storage capacitor V_{CS} and load V_{L} of the proposed circuit and the circuit shown in Fig. 8(a). Results show that the proposed circuit with EAI can power up the load more frequently than the circuit which uses a dc–dc converter as the interface between the storage capacitor and the load in a given time frame. The insets show that the proposed circuit can provide energy to the load for around 5 s with V_{L} equals V_{CS} and is between $V_{\text{CS,L}}$ and $V_{\text{CS,H}}$. The circuit shown in Fig. 8(a) can provide a constant voltage to the load but it lasts for less than 3 s even when most of the energy stored in the storage capacitor has been used, with V_{CS} drops to 0.4 V.

Still comparing both circuits, Fig. 12 shows the energy discharged by the storage capacitor and dissipated by the load. Within 150 s, the proposed circuit delivered 96% of the energy (185 mJ) from the capacitor to the load whereas only 78% of the energy (132 mJ) was transferred to the load by the circuit using two dc–dc converters. The proposed circuit also has a shorter idle time which allows energy to be transferred from the storage capacitor to the load more frequently, leading to a higher total energy transferred to the load. Therefore, the proposed circuit provides more useful energy from the
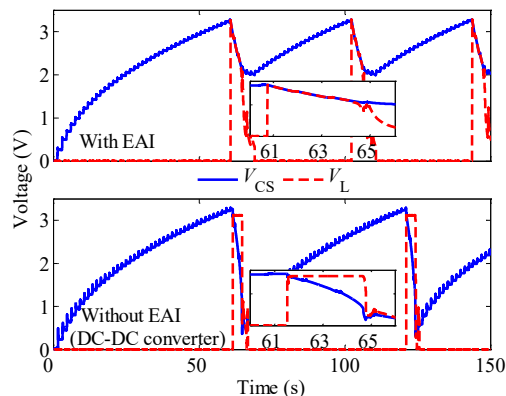

Fig. 11. Measured voltages at the storage capacitor (solid) and resistive load (dash) of the proposed circuit (top) and the circuit which uses a dc–dc converter (bottom) for energy flow management. The insets show the time duration of the load can be powered on using the different circuits.
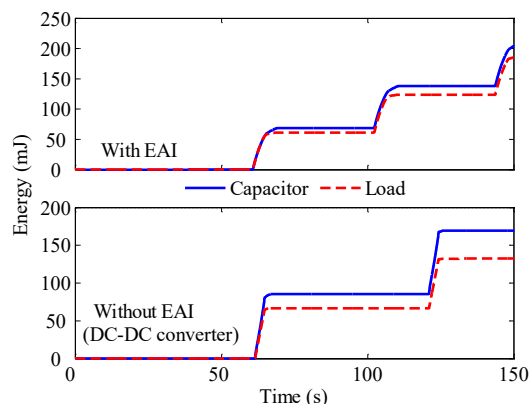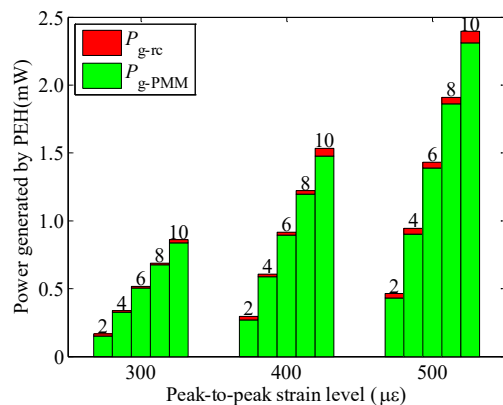

Fig. 12. Comparisons of the energy discharged by the storage capacitor (solid) and energy dissipated by the load (dash) in the two different circuit configurations mentioned in Fig. 11 over 150 s.

Fig. 13. Comparisons of the powers generated by the PEH which is connected to its optimal load ($P_{\text{g-rc}}$) and connected to the proposed circuit ($P_{\text{g-PMM}}$) to show the adaptability of the circuit in energy harvesting under various strain loadings and frequencies. The numbers above the bars represent frequency.
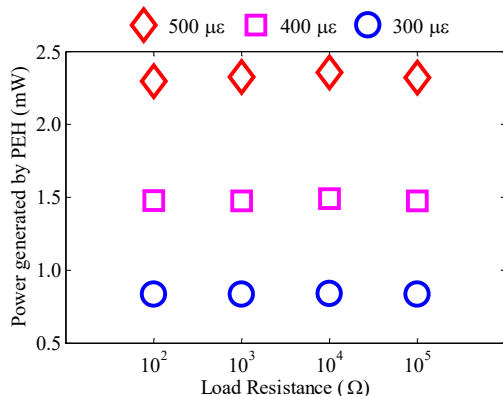

Fig. 14. Power generated by the PEH when connected with the developed circuit with different values of R_{L} under different strain loadings at 10 Hz.

harvester to the load.

B. Adaptability to Different Mechanical and Electrical Loads

Fig. 13 compares the powers generated by the PEH between the proposed circuit and the circuit shown in Fig. 8(b). The results show that power harvested from the PEH by the proposed power management circuit is close to the circuit which is connected with its optimal load under different applied strain loadings and frequencies. Fig. 14 also shows that the power generated by the PEH when connected to the developed power management circuit is not much influenced by the connected resistive load at the output of the power management circuit for all the tested conditions.

The proposed circuit was also used to power a WSN (LTC5800-WHM) to demonstrate that the circuit can be used in real-world applications. A peak-to-peak strain level of 500 µε at 10 Hz was applied to the PEH in the test. Fig. 15 shows the measured voltage at the storage capacitor and the current drawn by the WSN. The inset shows the enlarged view of the measured voltage and current. The circuit is capable of meeting the variable current loads demanded by the WSN for various tasks and processes. Since the WSN draws the energy out directly from the storage capacitor, the capacitor voltage decreases at a rate which is proportional to the current consumed.

From these tests, the proposed power management circuit is shown to be adaptive to the varying input from the energy harvester due to the variants of its surroundings. The performance is stable regardless of the connected load at the output of the circuit. This is attributed to the decoupling of the energy harvester and the load from the power management circuit whenever appropriate as discussed in Section V.A.

C. Power Consumption

The total power consumption of the proposed circuit is 66.11–590.83 µW under the tested conditions. Fig. 16 shows the breakdown of the power consumptions where P_{ACC} of the ACC and P_{EAI} of the EAI were calculated using (5) based on the measured voltages and currents while P_{FB} of the FB rectifier and P_{DCDC} of the dc–dc converter were obtained using (7) and (9), respectively. The majority of the power consumed and losses are from the FB rectifier and the dc–dc converter at 12.81–113.71 µW and 47.43–469.08 µW, respectively. The ACC and EAI which are the main functional blocks for the operation of the power management circuit have low power consumptions of around 5.16–6.78 µW and 0.705–1.26 µW, respectively. This is because of the simplicity of the circuitries as shown in Fig. 1, the simplicity of the operation as explained in Section II, and the choice of the components that are inherently low power. The low power consumption of the ACC and EAI enables the power management circuit to self-start without difficulty. Since the power consumption of a dc–dc converter is much higher than the EAI, the use of the EAI for energy flow management is justified, especially to allow more harvested energy available to the load such as WSNs that have a wide operating voltage range, unless a constant voltage is required by the load.
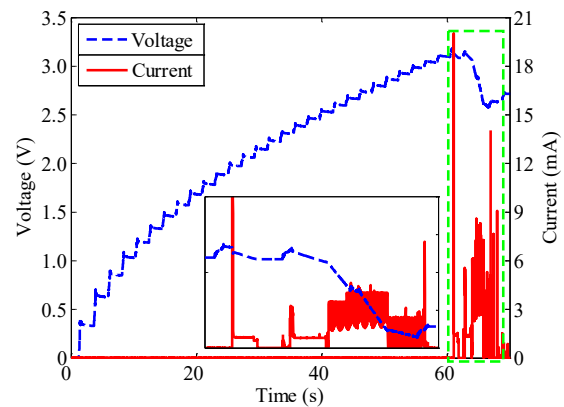

Fig. 15. Measured voltage at the storage capacitor (dashed) and current (solid) drawn out by a wireless sensor node that is powered by the proposed circuit. The inset shows the enlarged view of the area highlighted by the dashed line.
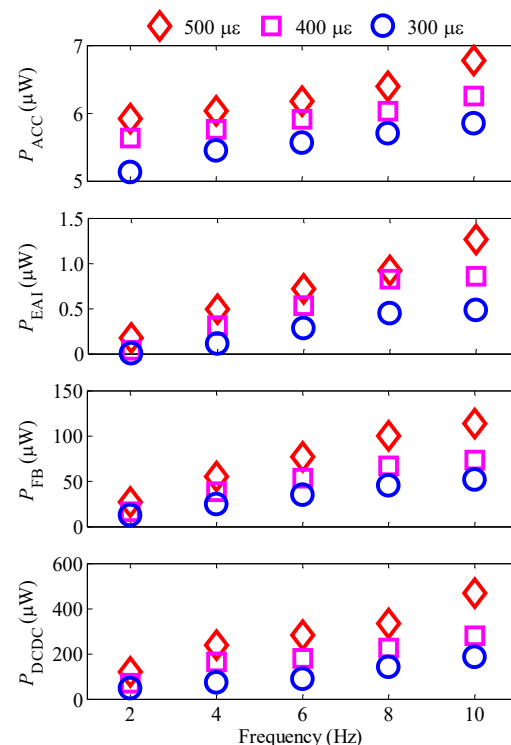

Fig. 16. Power consumptions and losses P_{ACC} of the analog control circuit, P_{EAI} of the EAI, P_{FB} of the FB rectifier, and P_{DCDC} of the dc–dc converter in the developed circuit when strain loadings of 300 µε (circle), 400 µε (square), and 500 µε (diamond) were applied onto the PEH at frequencies of 2 to 10 Hz.

It can be seen that all the power consumptions follow a similar trend which increases with both the strain loading and frequency applied onto the PEH. The smoothing capacitor can be charged up faster when strain loadings with higher frequencies were applied, and hence the occurrences of the MPP of the PEH also increase. This means the circuit is required to transfer the energy to the storage capacitor more often and also release the stored energy to the load more often when the storage capacitor can be charged up quicker, leading to an increase in the power consumption of the circuit.

Given that operation at high frequencies leads to higher power consumption as can be seen from the results in Fig. 16, the low power consumption of the ACC and EAI can also be explained in terms of their generally low frequency operation
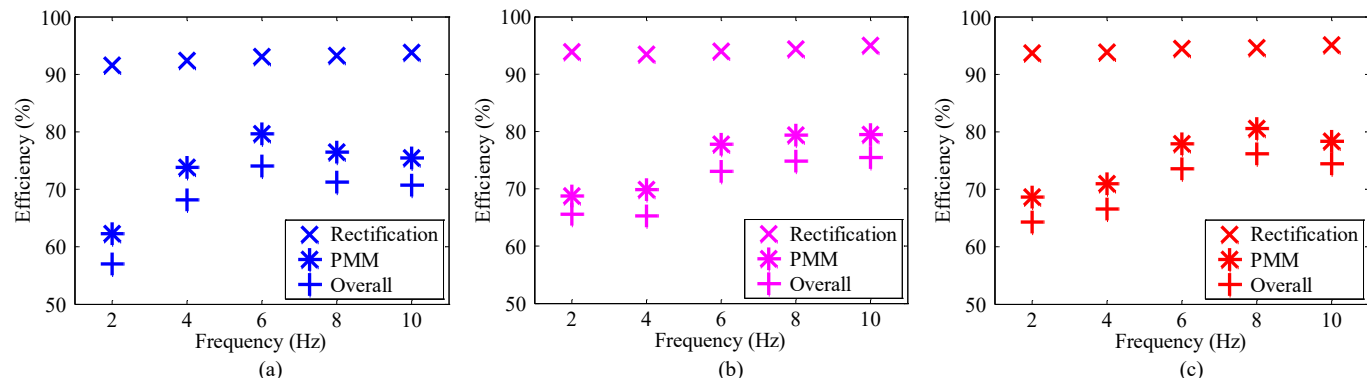
Fig. 17. Rectification efficiencies η_{rect}, PMM efficiencies η_{PMM}, and overall efficiencies $\eta_{overall}$ of the developed circuit in delivering the harvested power to the load with frequencies of 2 to 10 Hz and strain loadings of: (a) 300 µε, (b) 400 µε, and (c) 500 µε applied onto the PEH.

where the ACC generates pulses at a relatively low frequency and the EAI turns on or off the load at specific threshold voltages, which happens infrequently as can be seen in Fig. 10 and Fig. 11, respectively.

D. Efficiencies of the Overall System and Subsystems

Fig. 17 shows the efficiencies as calculated using (6), (8), and (10). The rectifier efficiency η_{rect} is 91.58% to 95.08%, showing that the use of simple FB rectifier is viable since the efficiency is quite high in the implemented circuit. The efficiency of the PMM η_{PMM} is around 78% for most cases with the peak efficiency at 80.58% but is slightly lower at low frequencies. As mentioned earlier, the time between successive energy transfers increases when the frequency decreases and vice versa. With the energy transfers become less frequent, the average output power P_{out} also reduces, and therefore reduces the efficiency. The overall efficiency of the circuit in transferring the energy from the PEH to the storage capacitor $\eta_{overall}$ follows the trend of η_{PMM} but is slightly lower than η_{PMM} as it includes the power dissipated at the FB rectifier. Therefore, $\eta_{overall}$ is around 74% in most cases with the peak at 76.18%, which occurs when the PEH was subjected to a peak-to-peak strain loading of 500 µε at 8 Hz.

VI. CONCLUSIONS

An adaptive power management circuit is presented where piezoelectric energy harvesting is used as a demonstration. The circuit is able to harvest and manage the power from a PEH which is subjected to variable frequencies and amplitudes of strain loadings and variable connected electric loads. The adaptiveness of the circuit is due to the operation of the subsystems which decouple the load from the energy harvester using the ACC, dc–dc converter, and the EAI. The decoupling process in the MPP finding and energy accumulation makes the energy harvester becomes less likely to be influenced by the connected load. Also, the maximum power transfer and energy flow as controlled by the ACC and the EAI respectively do not interfere with each other. The energy harvester is connected to the storage capacitor only momentarily at its MPP for energy transfer via the dc–dc converter as controlled by the ACC. The power management circuit is shown to be capable of harvesting power close to a reference circuit with its optimal load in the tested conditions. The EAI controls the energy flow to the load,

by allowing the energy to be drawn by the load directly from the storage capacitor only when there is sufficient energy for the load. The EAI is also more energy efficient than other interfaces such as dc–dc converters for a better use of the energy harvested and stored in the storage capacitor by the load where more energy can be transferred to the load. The power management circuit is able to self-start easily due to the low power consumption of the ACC and EAI, and achieves a peak overall efficiency in transferring energy from the PEH to the storage capacitor of up to 76.18%. Therefore, the presented circuit shows better utilization of the harvested energy than conventional circuit architecture in which more energy can be used by the load for meaningful task. This is particularly promising for real-world applications with WSNs powered by energy harvesting.

REFERENCES

[1] S. Sudevalayam, and P. Kulkarni, "Energy harvesting sensor nodes: Survey and implications," *IEEE Commun. Surv. Tut.,* vol. 13, no. 3, pp. 443-461, 2011.

[2] F. Federici, F. Graziosi, M. Faccio, A. Colarieti, V. Gattulli, M. Lepidi, and F. Potenza, "An integrated approach to the design of wireless sensor networks for structural health monitoring," *Int. J. Distrib. Sens.Netw.,* vol. 8, no. 3, pp. 594842 (16 pp), 2012.

[3] B. Martinez, M. Montón, I. Vilajosana, and X. Vilajosana, "Early scavenger dimensioning in wireless industrial monitoring applications," *IEEE Internet Things J.,* vol. 3, no. 2, pp. 170-178, 2016.

[4] M. K. Stojčev, M. R. Kosanović, and L. R. Golubović, "Power management and energy harvesting techniques for wireless sensor nodes," in *9th Int. Conf. TELSIKS*, 2009, pp. 65-72.

[5] D. Brunelli, "A high-efficiency wind energy harvester for autonomous embedded systems," *Sensors,* vol. 16, no. 3, pp. 327 (19 pp), 2016.

[6] A. Montecucco, and A. R. Knox, "Maximum power point tracking converter based on the open-circuit voltage method for thermoelectric generators," *IEEE Trans. Power Electron.,* vol. 30, no. 2, pp. 828-839, 2015.

[7] M. Shim, J. Kim, J. Jeong, S. Park, and C. Kim, "Self-powered 30 µW to 10 mW piezoelectric energy harvesting system with 9.09 ms/V maximum power point tracking time," *IEEE J. Solid-State Circuits,* vol. 50, no. 10, pp. 2367-2379, 2015.

[8] Y. K. Tan, and S. K. Panda, "Optimized wind energy harvesting system using resistance emulator and active rectifier for wireless sensor nodes," *IEEE Trans. Power Electron.,* vol. 26, no. 1, pp. 38-50, 2011.

[9] G. Chowdary, A. Singh, and S. Chatterjee, "An 18 nA, 87% efficient solar, vibration and RF energy-harvesting power management system with a single shared inductor," *IEEE J. Solid-State Circuits,* vol. 51, no. 10, pp. 2501-2513, 2016.

[10] M. Dini, A. Romani, M. Filippi, V. Bottarel, G. Ricotti, and M. Tartagni, "A nanocurrent power management IC for multiple heterogeneous energy

harvesting sources," *IEEE Trans. Power Electron.,* vol. 30, no. 10, pp. 5665-5680, 2015.

[11] D. Masotti, A. Costanzo, P. Francia, M. Filippi, and A. Romani, "A load-modulated rectifier for RF micropower harvesting with start-up strategies," *IEEE Trans. Microw. Theory Tech.,* vol. 62, no. 4, pp. 994-1004, 2014.

[12] N. Kong, and D.-S. Ha, "Low-power design of a self-powered piezoelectric energy harvesting system with maximum power point tracking," *IEEE Trans. Power Electron.,* vol. 27, no. 5, pp. 2298-2308, 2012.

[13] G. K. Ottman, H. F. Hofmann, A. C. Bhatt, and G. A. Lesieutre, "Adaptive piezoelectric energy harvesting circuit for wireless remote power supply," *IEEE Trans. Power Electron.,* vol. 17, no. 5, pp. 669-676, 2002.

[14] A. Tabesh, and L. G. Fréchette, "A low-power stand-alone adaptive circuit for harvesting energy from a piezoelectric micropower generator," *IEEE Trans. Ind. Electron.,* vol. 57, no. 3, pp. 840-849, 2010.

[15] P. Gasnier, J. Willemin, S. Boisseau, G. Despesse, C. Condemine, G. Gouvernet, and J. J. Chaillout, "An autonomous piezoelectric energy harvesting IC based on a synchronous multi-shot technique," *IEEE J. Solid-State Circuits,* vol. 49, no. 7, pp. 1561-1570, 2014.

[16] Z. J. Chew, and M. Zhu, "Adaptive maximum power point finding using direct $V_{\text{OC}}/2$ tracking method with microwatt power consumption for energy harvesting " *IEEE Trans. Power Electron.,* vol. 33, no. 9, pp. 8164-8173, 2018.

[17] J. Sather, "Battery technologies for IoT," *Enabling the internet of things: From integrated circuits to integrated systems*, 1 ed. M. Alioto, Ed. Springer International Publishing, 2017, ch. 15, pp. 409-440.

[18] T. Ruan, Z. J. Chew, and M. Zhu, "Energy-aware approaches for energy harvesting powered wireless sensor nodes," *IEEE Sensors J.,* vol. 17, no. 7, pp. 2165-2173, 2017.

[19] Z. J. Chew, T. Ruan, and M. Zhu, "Strain energy harvesting powered wireless sensor system using adaptive and energy-aware interface for enhanced performance," *IEEE Trans. Ind. Informat.,* vol. 13, no. 6, pp. 3006-3016, 2017.

[20] Z. J. Chew, and M. Zhu, "Threshold voltage control to improve energy utilization efficiency of a power management circuit for energy harvesting applications," *Proceedings,* vol. 2, no. 13, pp. 1052 (5 pp), 2018.

[21] Analog Devices, "LTC2934 – ultra-low power adjustable supervisor with power-fail output," Rep. no. LTC2934-1/2, Datasheet., 2008.

[22] E. Casilari, J. M. Cano-García, and G. Campos-Garrido, "Modeling of current consumption in 802.15.4/ZigBee sensor motes," *Sensors,* vol. 10, no. 6, pp. 5443-5468, 2010.

[23] A. Giuliano, and M. Zhu, "A passive impedance matching interface using a PC permalloy coil for practically enhanced piezoelectric energy harvester performance at low frequency," *IEEE Sensors J.,* vol. 14, no. 8, pp. 2773-2781, 2014.